ADVANCES IN ATMOSPHERIC SCIENCES, VOL. 40, FEBRUARY 2023, 223–234

• **Original Paper** •

Ground-Based Atmospheric CO_2, CH_4, and CO Column Measurements at Golmud in the Qinghai-Tibetan Plateau and Comparisons with TROPOMI/S5P Satellite Observations

Minqiang ZHOU*[1], Qichen NI[1,2], Zhaonan CAI*[1], Bavo LANGEROCK[3], Jingyi JIANG[4], Ke CHE[1,2], Jiaxin WANG[1,2], Weidong NAN[5], Yi LIU[1,2], and Pucai WANG[1,2]

[1]*Institute of Atmospheric Physics*, *Chinese Academy of Sciences*, *Beijing* 100029, *China*

[2]*University of Chinese Academy of Sciences*, *Beijing* 100049, *China*

[3]*Royal Belgian Institute for Space Aeronomy (BIRA-IASB)*, *Brussels* 1180, *Belgium*

[4]*The College of Forestry*, *Beijing Forest University*, *Beijing* 100091, *China*

[5]*Xianghe Observatory of Whole Atmosphere*, *Institute of Atmospheric Physics*, *Chinese Academy of Sciences*, *Langfang* 065499, *China*

(Received 21 April 2022; revised 1 July 2022; accepted 18 July 2022)

ABSTRACT

Measurements of carbon dioxide (CO_2), methane (CH_4), and carbon monoxide (CO) are of great importance in the Qinghai-Tibetan region, as it is the highest and largest plateau in the world affecting global weather and climate systems. In this study, for the first time, we present CO_2, CH_4, and CO column measurements carried out by a Bruker EM27/SUN Fourier-transform infrared spectrometer (FTIR) at Golmud (36.42ºE, 94.91ºN, 2808 m) in August 2021. The mean and standard deviation of the column-average dry-air mixing ratio of CO_2, CH_4, and CO (XCO_2, XCH_4, and XCO) are 409.3 ± 0.4 ppm, 1905.5 ± 19.4 ppb, and 103.1 ± 7.7 ppb, respectively. The differences between the FTIR co-located TROPOMI/S5P satellite measurements at Golmud are 0.68 ± 0.64% (13.1 ± 12.2 ppb) for XCH_4 and 9.81 ± 3.48% (–10.7 ± 3.8 ppb) for XCO, which are within their retrieval uncertainties. High correlations for both XCH_4 and XCO are observed between the FTIR and S5P satellite measurements. Using the FLEXPART model and satellite measurements, we find that enhanced CH_4 and CO columns in Golmud are affected by anthropogenic emissions transported from North India. This study provides an insight into the variations of the CO_2, CH_4, and CO columns in the Qinghai-Tibetan Plateau.

Key words: Ground-based FTIR, greenhouse gas, remote sensing, TROPOMI/S5P, Qinghai-Tibetan Plateau

Citation: Zhou, M. Q., and Coauthors, 2023: Ground-based atmospheric CO_2, CH_4 and CO column measurements at Golmud in the Qinghai-Tibetan Plateau, and comparisons with TROPOMI/S5P satellite observations. *Adv. Atmos. Sci.*, **40**(2), 223–234, https://doi.org/10.1007/s00376-022-2116-0.

Article Highlights:

- CO_2, CH_4, and CO columns were observed at Golmud in August 2021 with the mean values of 409.3 ppm, 1905.5 ppb, and 103.1 ppb, respectively.
- A high correlation between CH_4 and CO is observed by both ground-based FTIR and co-located TROPOMI/S5P satellite measurements.
- CH_4 and CO column enhancements at Golmud are affected by the anthropogenic emissions in North India.

1. Introduction

Carbon dioxide (CO_2), methane (CH_4), and carbon monoxide (CO) are important atmospheric trace gases that affect air quality and climate change (IPCC, 2013). To provide highly accurate and precise total column measurements of CO_2, CH_4, and CO, the Total Carbon Column Observing Network (TCCON) was established in 2004 and is continuously running today (Wunch et al., 2011). Currently, there are 28 operational sites worldwide covering the latitude range from 45ºS to 80ºN (https://tccondata.org/). The TCCON requires the Bruker IFS 125HR Fourier-transform infrared spectrometer (FTIR) to record direct solar absorption of near-infrared spectra. The Bruker 125HR spectrometer is

* Corresponding authors: Minqiang ZHOU, Zhaonan CAI
Emails: minqiang.zhou@mail.iap.ac.cn, caizhaonan@mail.iap.ac.cn

stable but difficult to move, and the instrument requires a full alignment when transported. To fill the gap in the TCCON measurements, the COllaborative Carbon Column Observing Network (COCCON, Frey et al., 2015), using well-calibrated portable FTIR spectrometers (such as the Bruker EM27/SUN), was established and developed in recent years. The dry-air column-averaged mole fractions of CO_2, CH_4, and CO (XCO_2, XCH_4, and XCO) retrievals from the portable FTIR have been compared to the TCCON measurements and co-located AirCore profiles at several sites. The results show that the XCO_2, XCH_4, and XCO columns retrieved from the EM27/SUN portable FTIR have similar precision compared to those from a 125HR measurement (Frey et al., 2019; Sha et al., 2020).

Due to its unique topography, the Qinghai-Tibetan Plateau (QTP) plays an important role in earth's climate system (Ge et al., 2017; Zhang et al., 2021). The extremely high mountains in the QTP can change the atmospheric thermodynamic and dynamic status and, therefore, make a fundamental impact on the Indian monsoon, Asian monsoon, and other climate and weather systems (Tada et al., 2016; Zhou et al., 2019). In addition, Bian et al. (2020) pointed out that the air pollutants near the surface in Asia can be transported to the stratosphere via the QTP, thereby allowing for global transport. Measurements of CO_2, CH_4, and CO in the QTP are of great importance for understanding the background of our planet. There are two sites in the QTP monitoring CO_2, CH_4, and CO concentrations near the surface (Guo et al., 2020; Liu et al., 2021). However, until now, there was no TCCON site in the QTP providing XCO_2, XCH_4, and XCO measurements. Compared to surface in situ measurements, column measurements are less affected by the change of the atmospheric planetary boundary layer thickness and are also less influenced by nearby point sources. Another advantage of the ground-based XCO_2, XCH_4, and XCO measurements is that they have a similar observation geometry to the satellite measurements. Therefore, column measurements serve as a better satellite validation reference than surface in situ measurements (Zhou et al., 2016; Wunch et al., 2017; Sha et al., 2021).

In this study, we present the EM27/SUN measurements carried out at Golmud [36.42ºE, 94.91ºN, 2808 m above sea level (a.s.l.)], Qinghai province, in August 2021. The EM27/SUN FTIR operated in Golmud is in line with COCCON measurement guidelines. To our knowledge, this is the first study showing the ground-based FTIR XCO_2, XCH_4, and XCO measurements in the QTP. The synoptic and diurnal variations of XCO_2, XCH_4, and XCO, and the correlations among these species, are discussed. After that, the EM27/SUN FTIR measurements are compared to the co-located TROPOMI/S5P satellite observations. The remainder of this paper is organized as follows. Section 2 describes the experimental site and observations, Section 3 presents the method, Section 4 discusses the results, and Section 5 provides conclusions.

2. Experiment site and observations

The near-infrared solar absorption spectra, with spectral coverage from 3900 to 11 000 cm^{-1} and a spectral resolution of 0.5 cm^{-1}, were recorded by a Bruker EM27/SUN FTIR (serial number 110; Hase et al., 2015) in the Golmud Meteorological Bureau. Surface temperature and pressure are continuously observed in the site next to the FTIR instrument. The site's location is shown in Fig. 1. Golmud is inside the QTP, and the surface altitude is 2808 m a.s.l. The landscape of this region is mainly grassland and bare areas (http://maps.elie.ucl.ac.be/CCI/viewer/index.php). In August 2021, the mean temperature was 18º Celsius, and the mean relative humidity was 32%. Golmud is a small city with a population of about 200 000. A large photovoltaic power station, situated about 20 km east of the Golmud city center, provides energy for the residents. Inside the city, there are no large factories, and the economic income mainly comes from animal husbandry, planting, and tourism. Figure 1 also shows the main roads and the rivers around Golmud, together with the CO_2 anthropogenic emissions from the Open-source Data Inventory for Anthropogenic CO_2 (ODIAC) inventories (Oda et al., 2018). The EM27/SUN site is located in the northern part of the city, marked by the blue star in Fig. 1.

The FTIR measurements were only operated during clear sky conditions. In total, we collected 21 days of EM27/SUN FTIR measurements in August 2021. There are about 600 spectra for each measurement day (between 1000 and 1900 local time (LST)), and one spectrum takes about 59 seconds to record. The FTIR XCO_2, XCH_4, and XCO retrievals are executed using the PROFFAST retrieval code, commonly used in the COCCON community (Frey et al., 2015; Tu et al., 2020; Sha et al., 2021). After the Golmud campaign, the EM27/SUN FTIR was shipped to Xianghe, Hebei Province, where we operated the EM27/SUN measurements next to a Bruker 125HR TCCON site between September and November 2021. To reduce the systematic uncertainty of the EM27/SUN FTIR retrievals, the EM27/SUN XCO_2, XCH_4, and XCO measurements have been scaled to the TCCON based on the co-located measurements collected at Xianghe (GGG2014; Wunch et al., 2015). The scaling factors of EM27/SUN XCO_2, XCH_4, and XCO used in this study are 1.002, 1.006, and 0.854, respectively. After scaling, the EM27/SUN FTIR retrievals deliver similar accuracy and precision as TCCON, which are 0.05 ± 0.25% (accuracy ± precision) for XCO_2, 0.10 ± 0.50% for XCH_4, and 3.0 ± 4.0% for XCO, respectively (Wunch et al., 2015).

We use the offline CH_4 and CO products from the TROPOspheric Monitoring Instrument (TROPOMI) onboard the S5P satellite (https://scihub.copernicus.eu/). The CH_4 columns are retrieved from the near infared (NIR: 0.76 μm) and shortwave infrared (SWIR 2.3 μm) bands (Hu et al., 2016), with a spatial resolution of 7.0 × 7.0 km^2 before 6 August 2019 and of 7.0 × 5.5 km^2, afterward. The latest CH_4 product has corrected the uncertainty attributed to the surface albedo (Lorente et al., 2021). The retrieval uncertainty of the TROPOMI XCH_4 meets its mission requirement with

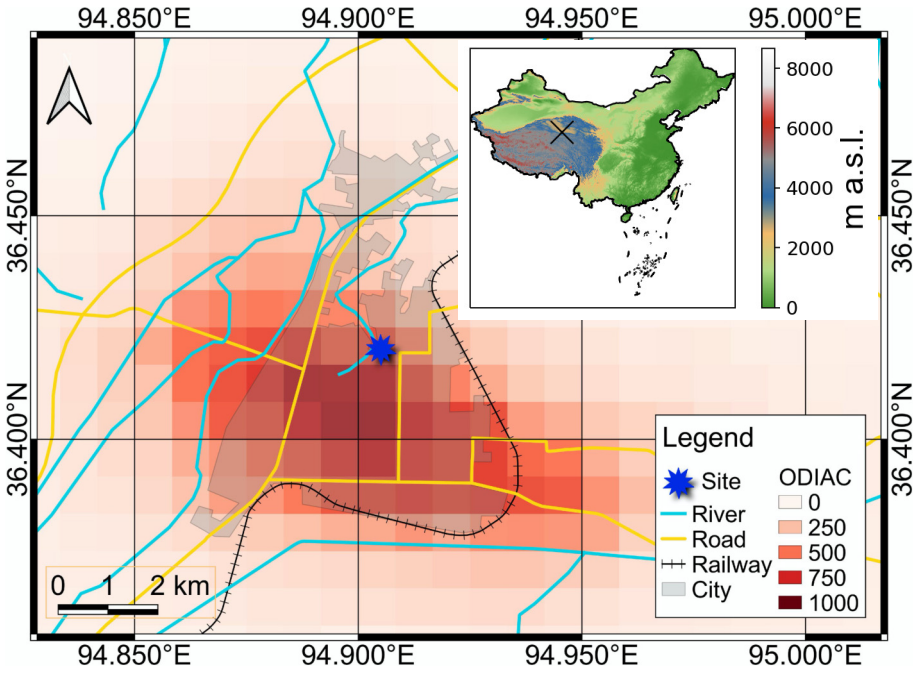

Fig. 1. The location of the EM27/SUN measurement site at Golmud. The map is colored with the anthropogenic CO_2 emissions from the ODIAC inventory. The ODIAC emissions correspond to the monthly mean of August 2019, with units of tonne carbon/cell (monthly total). Golmud is in the Qinghai-Tibetan Plateau with an elevation of 2808 m a.s.l.

a systematic error of 1.5% and a random error of 1.0%. The relative mean and standard deviation of the differences between TROPOMI XCH_4 data and 25 TCCON global sites (GGG2014) are 0.26% and 0.57% (Sha et al., 2021). The TROPOMI/S5P CO product is retrieved from the SWIR (2.3 μm) spectral range under clear-sky conditions (Landgraf et al., 2016). The spatial resolution of the S5P XCO observations is the same as the S5P XCH_4 observations. Since 1 July 2021, the CO and CH_4 cross-sections have been updated using the DLR Scientific Exploitation of Operational Missions - Improved Atmospheric Spectroscopy Databases (SEOM-IAS) spectroscopy (Borsdorff et al., 2019; Rodina et al., 2021). Moreover, the stripes of erroneous CO values have been corrected based on the fixed masked de-striping method (Borsdorff et al., 2019). The retrieval uncertainty of the TROPOMI XCO also meets its mission requirement of a systematic error of 15 % and a random error of 10%. The relative mean and standard deviation of the differences between TROPOMI XCO and TCCON (standard GGG2014) data are 9.22% and 5.36 %, respectively (Sha et al., 2021). For the CO and CH_4 overpass data, we selected the S5P measurements around 50 km around Golmud. The satellite overpass time is about 1430 LST. Regarding CO_2 satellite measurements, we use the Level 2 bias-corrected XCO_2 retrospective processing OCO-2 V10 lite version (Kiel et al., 2019). OCO-2 provides a high spatial resolution of < 3 km^2 per sounding, but only eight measurements are recorded along a narrow track. During this campaign, there was only one day (17 August 2021) with five OCO-2 satellite soundings available within 50 km around Golmud. As the satellite CO_2 measurements are quite limited, we mainly focus on the comparisons between the FTIR and S5P XCH_4 and XCO measurements.

3. Methods

The time series of XCO_2, XCH_4, and XCO are plotted based on the individual EM27/SUN FTIR retrievals. The correlations among these three species are investigated based on the individual retrievals and the daily means. The Pearson correlation coefficients are calculated between XCO_2 and XCO and between XCH_4 and XCO.

To check the diurnal variations of these species, the FTIR X_{gas} anomaly (ΔX_{gas}) is derived as

$$\Delta X_{gas} = X_{gas} \overline{\mathrm{Xday}}\,, \tag{1}$$

where X_{gas} is the FTIR XCO_2, XCH_4, or XCO retrievals, and $\left(\overline{\mathrm{Xday}}\right)$is the daily median.

Regarding the comparison between the FTIR and S5P measurements, we follow the method used for TCCON and S5P measurements described in Sha et al. (2021). The EM27/SUN retrieval is similar to TCCON retrieval, as they both keep the vertical shape unchanged and apply a profile scaling. The FTIR and S5P retrievals use different a priori profiles. The a priori profiles of CO_2, CH_4, and CO FTIR retrievals come from the atmospheric chemistry model GEOS-FPIT model (https://gmao.gsfc.nasa.gov/pubs/docs/Lucchesi571.pdf). Normally an FTIR a priori profile varies with time, but a fixed a priori profile is used for all FTIR retrievals on the same day. The a priori profiles of S5P

retrievals come from another 3-D atmospheric chemistry-transport model (TM5) monthly means. To reduce the uncertainty from different a priori profiles, the a priori profile of the S5P satellite retrieval (TM5 model) is used as the common prior (Rodgers and Connor, 2003). It is then gridded to the FTIR retrieval grid with a mass conservation equation (Langerock et al., 2015).

$$X'_{\mathrm{FTIR}} = X_{\mathrm{FTIR}} + \mathrm{PC}_{\mathrm{air}}(I - A_{\mathrm{FTIR}})(x_{\mathrm{a,S5P}} - x_{\mathrm{a,FTIR}}) , \quad (2)$$

where X_{FTIR} is the original FTIR retrieval, X'_{FTIR} is the FTIR retrieval using the S5P a prior as the a priori profile, $\mathrm{PC}_{\mathrm{air}}$ is the vertical profile of dry-air partial column, I is the unity vector, A_{FTIR} is the column averaging kernel in a unit of molecule cm^{-2} / molecule cm^{-2} , and $x_{\mathrm{a,S5P}}$ and $x_{\mathrm{a,FTIR}}$ are the S5P and FTIR a priori profiles, respectively. In addition, the pixel altitude correction is carried out to bring the FTIR and S5P measurements to the same surface altitude. The scaling factor (f) is calculated based on the different surface altitudes from the FTIR and S5P retrievals (see Appendix B in Sha et al., 2021):

$$X'_{\mathrm{S5P}} = f X_{\mathrm{S5P}} . \quad (3)$$

For each FTIR measurement, we select all the S5P measurements within a temporal window of ±1 hour and a spatial distance of 50 km. For all FTIR-S5P data pairs, we apply the a priori substitution on the FTIR retrievals and apply the altitude correction on the S5P retrievals. According to the topography, all the S5P footprints within 50 km around Golmud have a similar surface altitude as the EM27/SUN FTIR, leading to a f value close to 1.0. Finally, we average the S5P measurements ($\overline{X'_{\mathrm{S5P}}}$), and compare them to the FTIR retrieval using the common a priori profile (X'_{FTIR}).

In addition to the ground-based and space-based measurements, the backward simulations of the Lagrangian particle dispersion model FLEXPART v10.4 model (Pisso et al., 2019) is used to understand the sources of the air observed by the EM27/SUN and S5P measurements at Golmud. The FLEXPART model is driven by the NCEP Climate Forecast System Version 2 (CFSv2) data with a horizontal resolution of 0.5° × 0.5° and 64 vertical levels from the surface to 0.266 hPa (Saha et al., 2014). We release 20 000 air particles between 1300 and 1500 LST on each FTIR measurement day, and the backward time duration is set to 10 days.

4. Results and discussion

4.1. *Time series, correlations, and diurnal variations*

The time series and correlations of the EM27/SUN FTIR XCO_2, XCH_4, and XCO measurements in August 2021 at Golmud are shown in Fig. 2. The mean and standard deviation (std) of XCO_2, XCH_4, and XCO are 409.3 ± 0.4 ppm, 1905.5 ± 19.4 ppb, and 103.1 ± 7.7 ppb, respectively. The XCO_2 at Golmud is much more stable than the other two species. The ratios of the standard deviation to the mean are 0.1% for XCO_2, 1.0% for XCH_4, and 7.5% for XCO, respectively. A good correlation between XCH_4 and XCO is observed by the FTIR measurements with a statistically significant correlation coefficient (R) of 0.86 (p <

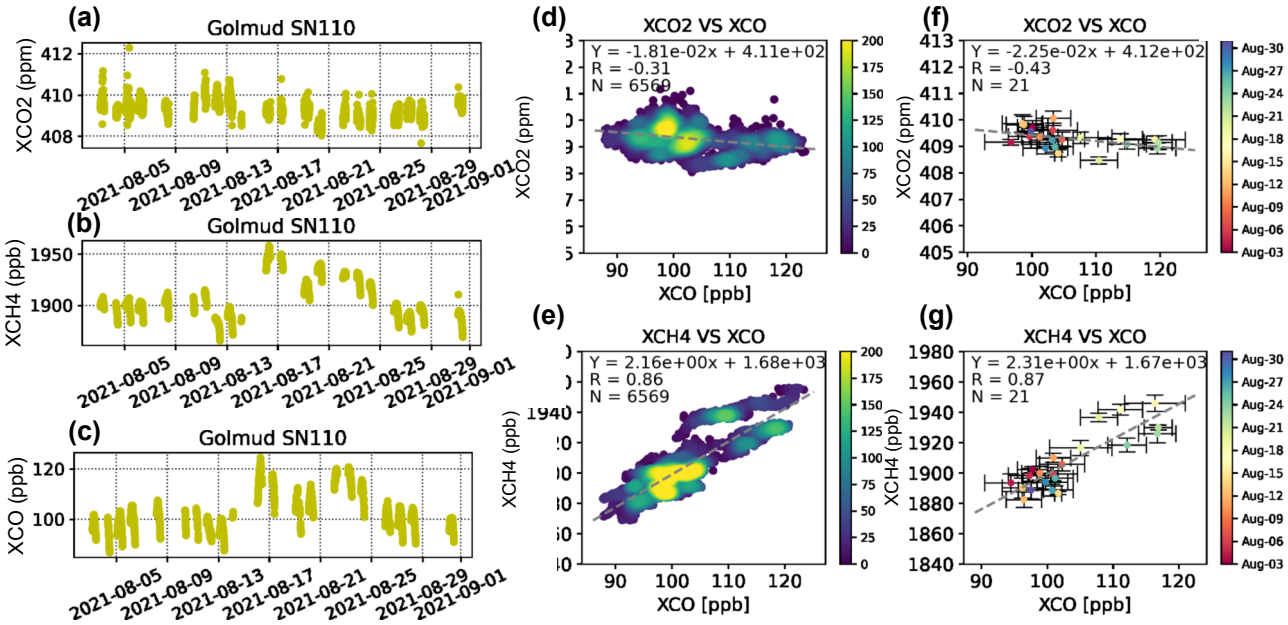

Fig. 2. The time series of the XCO_2 (a), XCH_4 (b), and XCO (c) from the EM27/SUN measurements in August 2021. Together with the correlation plots using the individual measurements between XCO and XCO_2 (d), and between XCO and XCH_4 (e), as well as the daily means between XCO and XCO_2 (f), and between XCO and XCH_4 (g). In (d) and (e), the dots are colored with the number densities. In (f) and (g), the error bars are the standard deviation of the measurements on that day, and the dots are colored with the measurement dates. The grey dashed line is the linear regression. The R-value is the Pearson correlation coefficient, and N is the number of dots.

0.05), whether derived from the 6569 individual measurements or 21 daily means. The enhancements of XCH_4 and XCO are observed simultaneously between 16 and 24 August, with two peaks around 16 August and 22 August. However, we do not observe an enhancement from the FTIR XCO_2 measurements between 16 and 22 August. The *R*-values between XCO_2 and XCO are –0.31 for the individual measurements and –0.43 for the daily means.

The ΔX_{gas} values over the 21 days are plotted together in Figs. 3a–c. It can be seen that ΔX_{gas} is generally higher at noon than in the morning and afternoon. Before interpreting the diurnal variation of ΔX_{gas}, we must access the influence from the smoothing uncertainty. According to Rodgers (2000), the retrieved X_{gas} can be written as

$$X_{gas} = X_{a,gas} + A\mathrm{PC}_{air}(x_t - x_a) + \varepsilon\,, \tag{4}$$

where $X_{a,gas}$ is the a priori dry-air column-averaged mole fraction, A is the column averaging kernel, x_t and x_a are the true and a priori gas profiles, and ε is the retrieval uncertainty. Due to the change of the light path during the day, the column averaging kernel, A, varies with the solar zenith angle (SZA, Fig. 3e). The typical averaging kernel of EM27 FTIR retrievals can be found in Hedelius et al. (2016). According to Eq. (4), even if the x_t is unchanged during a given day, the X_{gas} will vary with the SZA, leading to an artificial diurnal variation. To access the impact of the smoothing uncertainty on the diurnal variation, we use the Copernicus Atmosphere Monitoring Service (CAMS) model as the true status of atmospheric CO_2, CH_4, and CO at Golmud. Therefore, the difference between the CAMS model and retrieved X_{gas} becomes:

$$\begin{aligned}\mathrm{Diff}X_{gas} &= X_{cams} - X_{gas}\\ &= \mathrm{PC}_{air}x_{cams} - \left[X_{a,gas} + A\mathrm{PC}_{air}(x_{cams} - x_a)\right]\\ &= (I - A)\mathrm{PC}_{air}(x_{cams} - x_a)\,.\end{aligned} \tag{5}$$

Figure 4 shows $\mathrm{Diff}X_{gas}$ for CO_2, CH_4, and CO from all FTIR measurement days. Between 1000 and 1800 LST, the absolute $\mathrm{Diff}XCO_2$ is less than 0.05 ppm, $\mathrm{Diff}XCH_4$ is less than 0.5 ppb, and DiffXCO is less than 0.1 ppb. When the SZA is large (e.g., >60°), the smoothing error becomes significant, especially for XCO_2. Figure 3a shows that XCO_2 is high before 1000 and after 1800 LST, which is probably due to its large smoothing error with the large SZA (Fig. 4a).

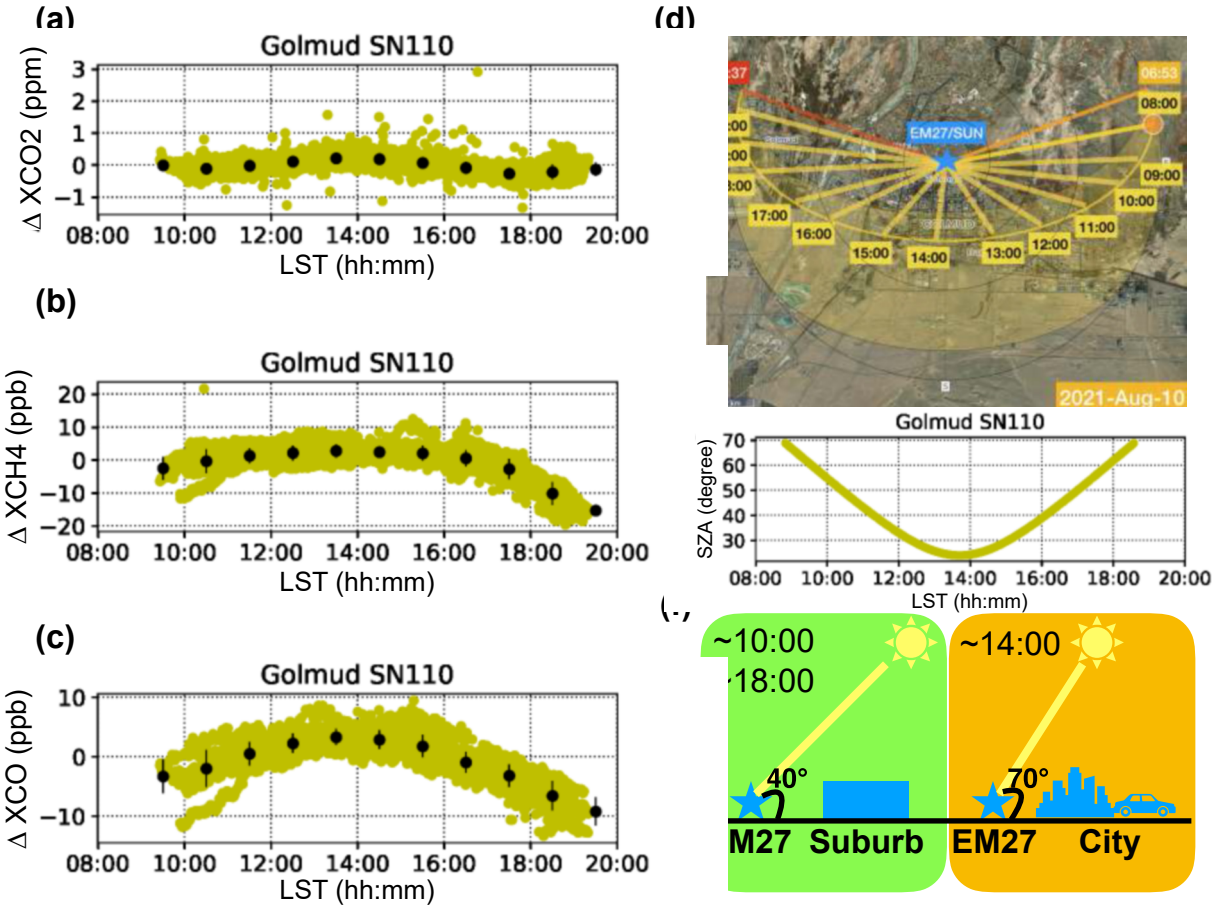

Fig. 3. The diurnal variations of ΔXCO_2 (a), ΔXCH_4 (b), and ΔXCO (c) as derived from the EM27/SUN measurements at Golmud in August 2021. The black dots and error bars are the hourly means and standard deviations of ΔX_{gas}. The solar light paths for each hour on 10 August 2021 with the city map from Google are illustrated in (d) along with the solar zenith angles (e). The geometric information of the EM27/SUN measurements in the morning or afternoon (~1000 and ~1800 LST) and for local noon (~1400 LST) is shown in (f).

It is notable that the CAMS model simulations are not the true atmospheric status. Therefore, the real smoothing uncertainty could potentially be even larger than our estimations. Regardless, based on our estimations, the smoothing errors of FTIR XCO_2, XCH_4, and XCO retrievals, with an SZA < 60º, are generally negligible.

The differences between the gas column at local noon (1300–1500 LST) and in the morning/afternoon (1000–1100 and 1700–1800 LST) are 0.38 ppm for XCO_2, 3.49 ppb for XCH_4, and 6.56 ppb for XCO, respectively. These differences are much larger compared to our estimated smoothing errors. Figures 3d and 3f show the geometric information of the EM27/SUN measurements in the morning (~1000 LST) or afternoon (~1800 LST) and at local noon (1300–1500 LST). The FTIR site is located in the northern part of the city. In the morning and afternoon, the sunlight passes over the suburbs. While, at the local noon, the sunlight passes above the city center. Since the anthropogenic emissions (residential consumption, transport, and other human activities) of these species are higher inside the city than in the suburbs, the FTIR measurements would be expected to show maximums for these species around local noon.

4.2. *Comparison with TROPOMI/S5P satellite measurements*

Figure 5 shows the time series of the co-located FTIR and TROPOMI/S5P satellite XCH_4 and XCO measurements, together with their correlations. The relative mean and standard deviation of the differences between the FTIR and STP ((SAT–FTIR)/(FTIR × 100%)) are 0.68% ± 0.64% (13.1 ± 12.2 ppb) for XCH_4 and –9.81% ±3 .48% (–10.7 ± 3.8 ppb) for XCO, respectively. Good correlations between the FTIR and S5P co-located measurements are found for both XCH_4 and XCO, with statistically significant R-values of 0.86 for both species (p< 0.05). Similar to the FTIR measurements, the co-located S5P measurements also show the enhancements of XCH_4 and XCO between 16 and 24 August.

The difference between the EM27 FTIR and S5P XCH_4 measurements is within the S5P mission requirements, with a systematic error of 1.5% and a random error of 1.0%. The difference between XCH_4 retrievals from FTIR and S5P at Golmud is generally consistent with TCCON measurements

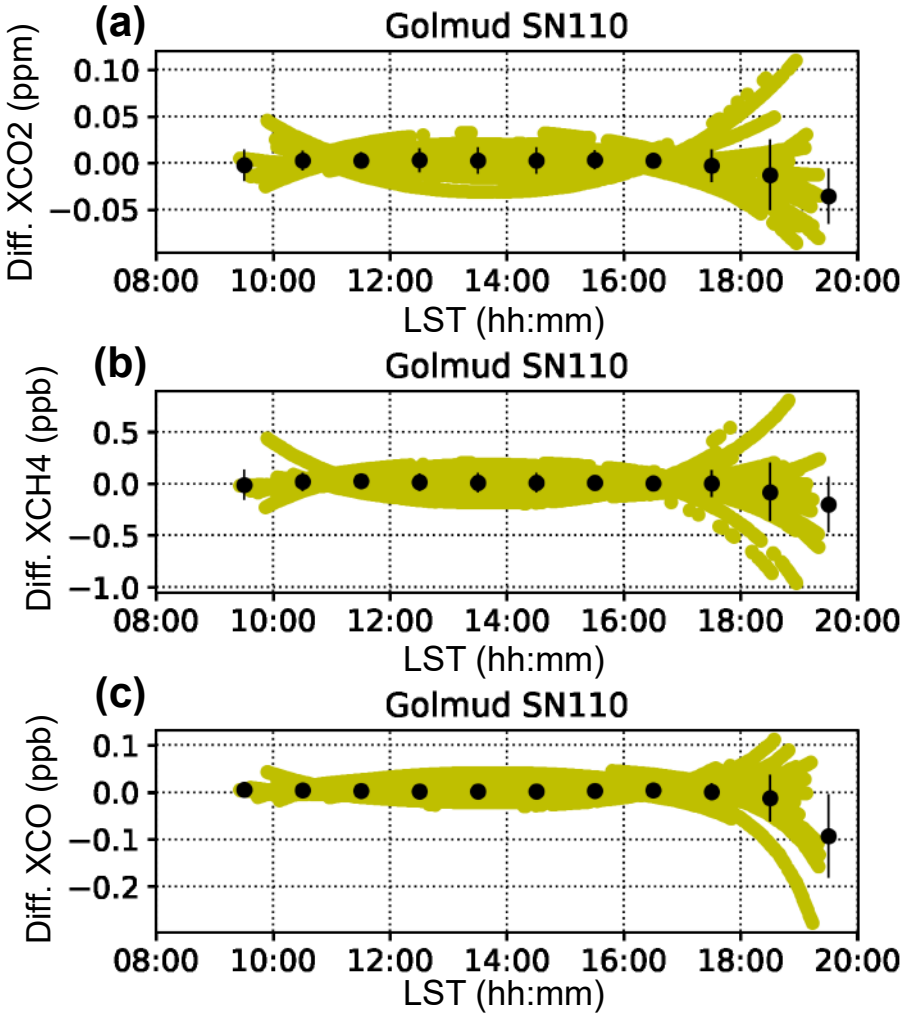

Fig. 4. The difference between the true XCO_2, XCH_4, and XCO (CAMS model) and the EM27/SUN FTIR retrievals using the GEOS-FPIT model as the a priori profile.

against the S5P XCH_4 data in Sha et al. (2021). It is notable that the impact coming from the different a priori profiles between the FTIR and S5P retrievals is small, as the mean difference between original EM27/SUN FTIR XCH_4 retrievals and the corrected FTIR retrievals using the S5P a priori as the common prior is –0.6 ppb (<0.1%). The reason is that TCCON and S5P a priori profiles are close to each other at Golmud. The standard deviation of S5P XCH_4 measurements (Fig. 5a) indicates that the uncertainty of the S5P retrieval in this region is high. Many satellite pixels are also filtered out in this region. Thus, we cannot identify a high XCH_4 value inside the Golmud city from the S5P monthly mean measurements (Fig. 6a).

The difference between EM27 FTIR and S5P XCO measurements is also within the S5P mission requirements, with a systematic error of 15% and a random error of 10%. However, the difference between TCCON and co-located S5P XCO measurements at Xianghe is only 2.05% ± 7.82% as reported by Yang et al. (2020), and –0.73% ± 7.35%, as reported by Sha et al. (2021), while the EM27/SUN FTIR

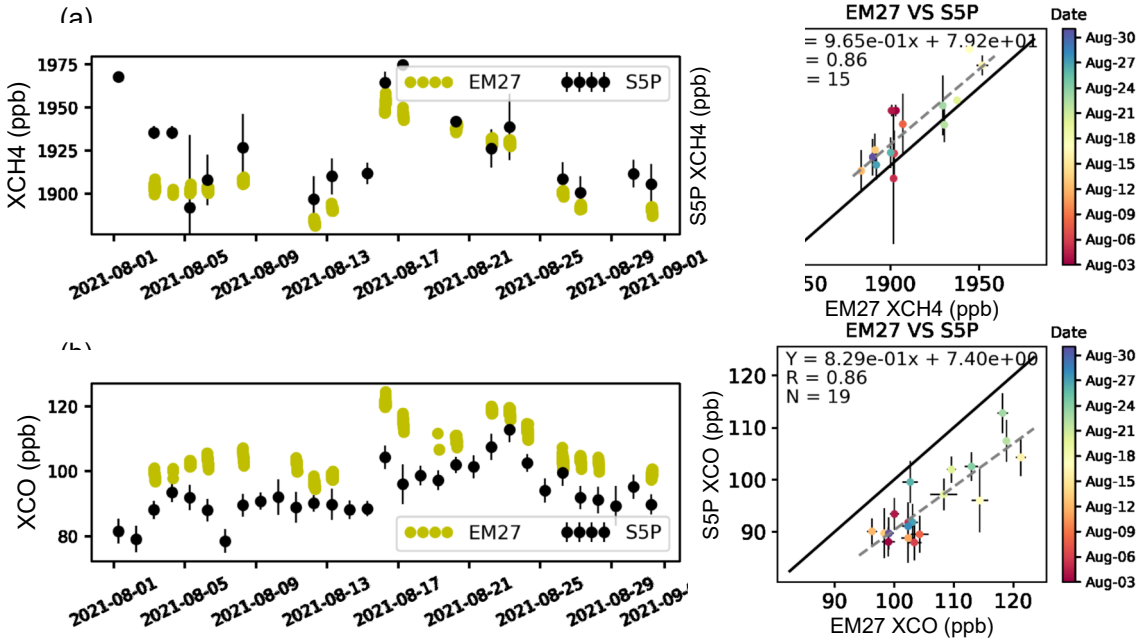

Fig. 5. The time series of the S5P XCH_4 (a) and XCO (b) satellite measurements plotted along with the co-located EM27/SUN FTIR measurements. The black error bars represent the standard deviation of all TROPOMI/S5P satellite measurements within 50 km around the site. Correlations are shown between the EM27/SUN and TROPOMI/S5P measurements for XCH_4 (c) and XCO (d). The error bars are the standard deviation of the co-located measurements on that day, and the dots are colored with the measurement dates. The solid black line is the one-to-one line, and the dashed grey line is the linear regression. The Pearson correlation coefficient is indicated by R, and N is the number of co-located days.

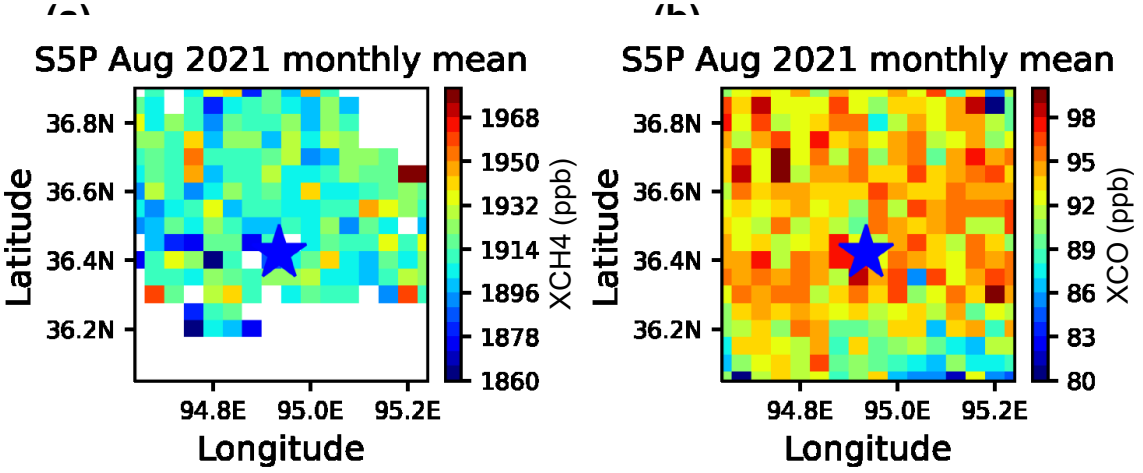

Fig. 6. The monthly means of the TROPOMI/S5P XCH_4 (a) and XCO (b) measurements around Golmud (blue star). The S5P data are binned into 0.05° × 0.05°.

measurement at Golmud is 9.81% ± 3.48% larger than the co-located S5P data. The large positive bias at Golmud is partially attributed to the different samplings between FTIR and S5P measurements. As mentioned above, the EM27 measurements observe the air above the Golmud city center during the S5P overpass time, while S5P measurements look at the regional mean within a distance of 50 km around the site. The monthly mean of S5P XCO measurements (Fig. 6b) can identify an XCO high value inside the Golmud city, with an increase of 4.3 ppb. In addition, the latest S5P satellite XCO product uses an updated spectroscopy product (from HITRAN2008 to SEOM-IAS) starting from 1 July 2021. The S5P retrievals using the updated spectroscopy can make XCO decrease by about 2.8 ppb (Borsdorff et al., 2019). If we consider both the sampling uncertainty and updated spectroscopy, the difference between the S5P and EM27/SUN FTIR XCO measurements at Golmud reduces to –3.6 ± 3.8 ppb.

4.3. *Airmass sources on the FTIR measurement days*

The FTIR and co-located S5P measurements both observed enhancements of XCH_4 and XCO between 16 and 24 August. When using the measurements before 16 August and after 24 August as the background, the amplitudes of the enhanced XCH_4 and XCO between 16 and 24 August were 41.6 ppb and 14.4 ppb, respectively. The amplitudes of the synoptic variations of XCH_4 and XCO are larger than the amplitudes of their diurnal variations. Figure 7 shows the FLEXPART 10-day backward trajectories for air particles released in the vertical range between the surface and 2 km above ground level (a.g.l.) over Golmud. The vertical range between the surface and 2 km is selected since the planetary boundary layer height at Golmud is about 2 km at 1400 LST, as indicated by the European Centre for Medium-Range Weather Forecasts (ECMWF) ERA5 hourly reanalysis data. Based on the co-located FTIR and S5P measurements shown in Fig. 5, we selected two days with an XCH_4 peak of 1951.9 ppb and XCO peak of 121.2 ppb on 16 August, and an XCH_4 peak of 1930.4 ppb and XCO peak of 118.9 ppb on 22 August. For the background, we select two days with a low XCO and XCH_4, where the XCH_4 means are 1883.5 ppb and 1900.2 ppb, and the XCO means are 96.7 ppb and 102.9 ppb on 12 and 26 August, respectively.

The spatial distributions of the backward trajectories on 12 and 26 August are similar, where air mass sources mainly come from the west and north. Different from the background cases, the airmass observed at Golmud came partly from the south (North India) on 16 and 22 August, with two different pathways: 1) air particles were directly transported from North India to Golmud and passed the Tibet plateau on 16 August; 2) air particles were transported along the Himalayas mountains from North India to the west north China (southern Xinjiang), and then transported to Golmud on 22 August. The two different air pathways on 16 August and 22 August are confirmed by the TROPOMI/S5P monthly XCO anomaly (ΔXCO = XCO – XCO monthly mean; Fig. 8). On 16 August, high ΔXCO values were observed in Tibet, indicating that the high XCO air particles mainly came from the south. On 22 August, high ΔXCO values were observed in southern Xinjiang, and ΔXCO was negative in Tibet, indicating that the high XCO observed in Golmud came from the west. In summary, the S5P monthly XCO anomaly measurements agree well with the FLEXPART backward simulations. According to the OCO-2 and S5P satellite measurements, we calculate the annual means of XCO_2, XCH_4, and XCO for middle and South Asia (Fig. 9). The XCH_4 and XCO in North India are much larger than in surrounding regions, the advection of which explains the high XCO and XCH_4 observed at Golmud on 16 and 22 August 2021. In addition, no clear high values of XCO_2 are found in North India compared to surrounding areas. Consequently, no XCO_2 enhancement is observed by the FTIR measurements during this period.

5. Conclusions

A Bruker EM27/SUN spectrometer provided atmospheric CO_2, CH_4, and CO column measurements at Golmud in August 2021. The means and standard deviations of XCO_2, XCH_4, and XCO are 409.3 ± 0.4 ppm, 1905.5 ± 19.4 ppb, and 103.1 ± 7.7 ppb, respectively. A high correlation between XCH_4 and XCO with an R of 0.86 is observed by the FTIR measurements. In addition, the diurnal variations of XCO_2, XCH_4, and XCO are derived from the FTIR measurements, with high values at local noon and low values in the early morning and late afternoon. The amplitudes of the diurnal variations are 0.38 ppm for XCO_2, 3.49 ppb for XCH_4, and 6.56 ppb for XCO, respectively. The similar diurnal variation, with a high value at local noon and low values in early morning and late afternoon, is observed for all three species, likely attributed to the observational geometry of the FTIR measurement. As the FTIR site is located in the northern part of the city, the FTIR observes the air mass above the suburbs in the morning and afternoon and observes the air mass above the city center at noon.

The EM27/SUN FTIR measurements at Golmud are also compared to the co-located S5P satellite measurements. The relative means and standard deviations of the differences between the FTIR and TROPOMI/S5P are 0.68% ± 0.64% for XCH_4 and –9.81 ± 3.48% for XCO, respectively. The difference between the FTIR and TROPOMI/S5P at Golmud generally agrees with previous validation studies at other places (Sha et al., 2021). The relatively high bias (–9.81%) in XCO is affected by the sampling mismatch between FTIR and TROPOMI/S5P, as well as the change in the spectroscopy updated by the TROPOMI/S5P CO retrieval algorithm (Borsdorff et al., 2019). The ground-based FTIR measurements in Golmud add to our knowledge about background greenhouse gas concentration in the Tibetan Plateau and also confirm the accuracy of satellite retrievals in this region. Currently, however, we only have one site covering one month in summer at Golmud. In the future, more ground-based FTIR measurements are needed to better under-

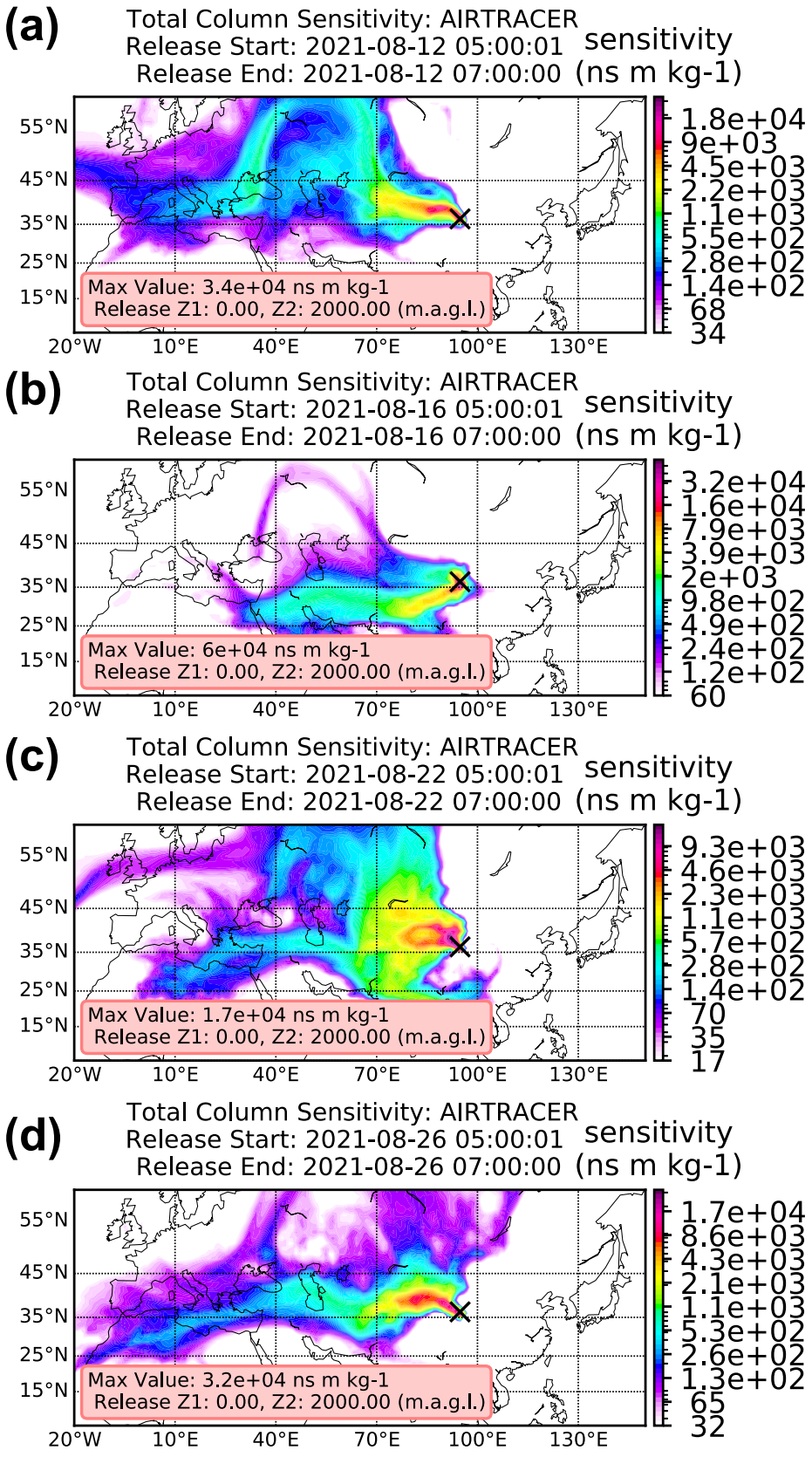

Fig. 7. The backward trajectories of the air mass at Golmud (black cross) in the vertical range between the surface and 2 km a.g.l. on 12 August (a), 16 August (b), 22 August (c), and 26 August (d) 2021, as simulated by a 10-day backward trajectory analysis using the FLEXPART model.

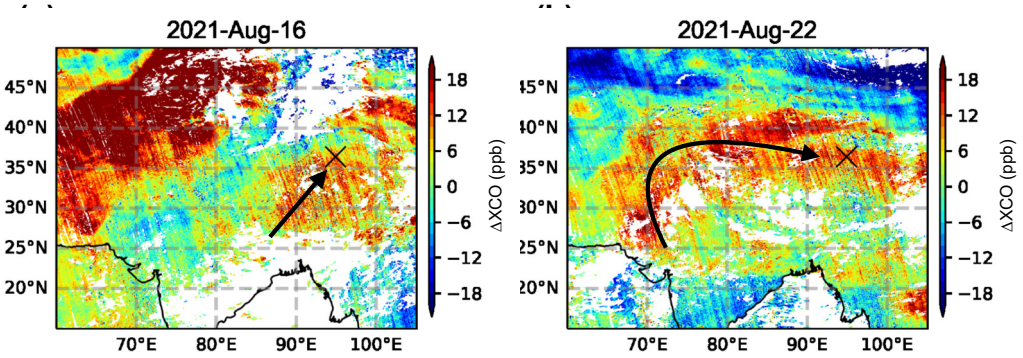

Fig. 8. The TROPOMI/S5P satellite monthly XCO anomaly (ΔXCO: XCO subtracted from the XCO monthly mean in August 2021) over the Qinghai-Tibetan Plateau on 16 August (a) and 22 August 2021 (b). The black arrow indicates the wind flow as shown by the FLEXPART simulations. The black cross represents the Golmud site.

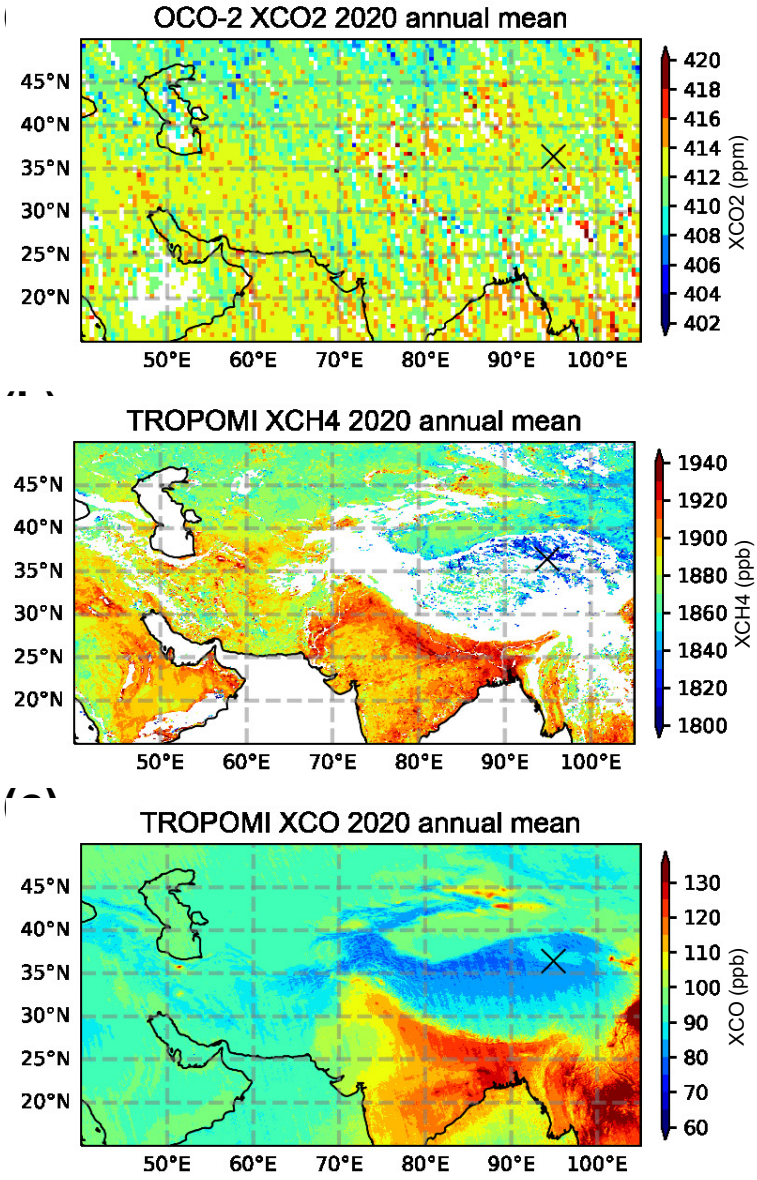

Fig. 9. The 2020 annual means of XCO_2 (a) observed by OCO-2 satellite measurements; and XCH_4 (b) and XCO (c) observed by the TROPOMI/S5P satellite measurements. The black cross represents the Golmud site.

stand the variations of XCO_2, XCH_4, and XCO in the QTP region and validate satellite greenhouse gas measurements in different seasons.

High correlations between the FTIR and S5P co-located measurements are found for both XCH_4 and XCO, with R values of 0.86 for both species. Moreover, enhancements of XCH_4 and XCO between 16 and 24 August are observed by both FTIR and S5P measurements. Based on the FTIR measurements, the amplitudes of the enhanced XCH_4 and XCO are 41.6 ppb and 14.4 ppb, respectively, which are larger than the amplitudes of their diurnal variations. The FLEXPART backward analysis show that the air mass during the enhancement period partly comes from North India. The S5P measurements confirm that the XCH_4 and XCO in India are much larger than in surrounding areas. It is inferred that the enhancements of the CH_4 and CO columns in Golmud are affected by the anthropogenic emissions transported from North India.

Acknowledgements. This research has been supported by the National Natural Science Foundation of China (Grant No. 42205140, 41975035) and the National Key Research and Development Program of China (2021YFB3901000). The authors would like to thank the ESA for providing the TROPOMI/S5P CH_4 and CO satellite data and NASA for providing the OCO-2 CO_2 satellite data. In addi- tion, the authors would like to thank Qun CHENG and Qing YAO for performing the TCCON and EM27/SUN measurements at Xianghe and the local support from the Golmud Meteorological Bureau.

REFERENCES

Bian, J. C., D. Li, Z. X. Bai, Q. Li, D. R. Lyu, and X. J. Zhou, 2020: Transport of Asian surface pollutants to the global stratosphere from the Tibetan Plateau region during the Asian summer monsoon. *National Science Review*, **7**, 516–533, https://doi.org/10.1093/nsr/nwaa005.

Borsdorff, T., and Coauthors, 2019: Improving the TROPOMI CO data product: Update of the spectroscopic database and destriping of single orbits. *Atmospheric Measurement Techniques*, **12**, 5443–5455, https://doi.org/10.5194/amt-12-5443-2019.

Frey, M., and Coauthors, 2015: Calibration and instrumental line shape characterization of a set of portable FTIR spectrometers for detecting greenhouse gas emissions. *Atmospheric Measurement Techniques*, **8**, 3047–3057, https://doi.org/10.5194/amt-8-3047-2015.

Frey, M., and Coauthors, 2019: Building the COllaborative carbon column observing network (COCCON): Long-term stability and ensemble performance of the EM27/SUN Fourier transform spectrometer. *Atmospheric Measurement Techniques*, **12**, 1513–1530, https://doi.org/10.5194/amt-12-1513-2019.

Ge, F., F. Sielmann, X. H. Zhu, K. Fraedrich, X. F. Zhi, T. Peng, and L. Wang, 2017: The link between Tibetan Plateau monsoon and Indian summer precipitation: A linear diagnostic perspective. *Climate Dyn.*, **49**, 4201–4215, https://doi.org/10.1007/s00382-017-3585-1.

Guo, M. R., and Coauthors, 2020: Comparison of atmospheric CO_2, CH_4, and CO at two stations in the Tibetan Plateau of China. *Earth and Space Science*, **7**, e2019EA001051, https://doi.org/10.1029/2019EA001051.

Hase, F., and Coauthors, 2015: Application of portable FTIR spectrometers for detecting greenhouse gas emissions of the major city Berlin. *Atmospheric Measurement Techniques*, **8**, 3059–3068, https://doi.org/10.5194/amt-8-3059-2015.

Hedelius, J. K., and Coauthors, 2016: Assessment of errors and biases in retrievals of X_{CO_2}, X_{CH_4}, X_{CO}, and X_{N2O} from a 0.5 cm^{-1} resolution solar-viewing spectrometer. *Atmospheric Measurement Techniques*, **9**, 3527–3546, https://doi.org/10.5194/amt-9-3527-2016.

Hu, H. L., and Coauthors, 2016: The operational methane retrieval algorithm for TROPOMI. *Atmospheric Measurement Techniques*, **9**, 5423–5440, https://doi.org/10.5194/amt-9-5423-2016.

IPCC, 2013: *Climate change 2013: The physical science basis. Contribution of Working Group I to the Fifth Assessment Report of the Intergovernmental Panel on Climate Change*, Cambridge University Press, Cambridge, United Kingdom and New York, NY, USA.

Kiel, M., C. W. O'Dell, B. Fisher, A. Eldering, R. Nassar, C. G. MacDonald, and P. O. Wennberg, 2019: How bias correction goes wrong: Measurement of X_{CO_2} affected by erroneous surface pressure estimates. *Atmospheric Measurement Techniques*, **12**, 2241–2259, https://doi.org/10.5194/amt-12-2241-2019.

Landgraf, J., and Coauthors, 2016: Carbon monoxide total column retrievals from TROPOMI shortwave infrared measurements. *Atmospheric Measurement Techniques*, **9**, 4955–4975, https://doi.org/10.5194/amt-9-4955-2016.

Langerock, B., M. De Mazière, F. Hendrick, C. Vigouroux, F. Desmet, B. Dils, and S. Niemeijer, 2015: Description of algorithms for co-locating and comparing gridded model data with remote-sensing observations. *Geoscientific Model Development*, **8**, 911–921, https://doi.org/10.5194/gmd-8-911-2015.

Liu, S., and Coauthors, 2021: Changes of atmospheric CO_2 in the Tibetan Plateau from 1994 to 2019. *J. Geophys. Res.*, **126**, e2021JD035299, https://doi.org/10.1029/2021JD035299.

Lorente, A., and Coauthors, 2021: Methane retrieved from TROPOMI: improvement of the data product and validation of the first 2 years of measurements. *Atmospheric Measurement Techniques*, **14**, 665–684, https://doi.org/10.5194/amt-14-665-2021.

Oda, T., S. Maksyutov, and R. J. Andres, 2018: The open-source data inventory for anthropogenic CO_2, version 2016 (ODIAC2016): A global monthly fossil fuel CO_2 gridded emissions data product for tracer transport simulations and surface flux inversions. *Earth System Science Data*, **10**, 87–107, https://doi.org/10.5194/essd-10-87-2018.

Pisso, I., and Coauthors, 2019: The Lagrangian particle dispersion model FLEXPART version 10.4. *Geoscientific Model Development*, **12**, 4955–4997, https://doi.org/10.5194/gmd-12-4955-2019.

Rodgers, C. D., 2000: *Inverse Methods for Atmospheric Sounding: Theory and Practice*. World Scientific Publishing Co. Pte. Ltd, https://doi.org/10.1142/3171.

Rodgers, C. D., and B. J. Connor, 2003: Intercomparison of remote sounding instruments. *J. Geophys. Res.*, **108**, 4116, https://doi.org/10.1029/2002JD002299.

Rodina, A. A., and Coauthors, 2021: Improved line list of $^{12}CH_4$ in the 4100–4300 cm^{-1} region. *Journal of Quantitative Spec-*

troscopy and Radiative Transfer, **279**, 108021, https://doi.org/10.1016/j.jqsrt.2021.108021.

Saha, S., and Coauthors, 2014: The NCEP climate forecast system version 2. *J. Climate*, **27**, 2185–2208, https://doi.org/10.1175/JCLI-D-12-00823.1.

Sha, M. K., and Coauthors, 2020: Intercomparison of low- and high-resolution infrared spectrometers for ground-based solar remote sensing measurements of total column concentrations of CO_2, CH_4, and CO. *Atmospheric Measurement Techniques*, **13**, 4791–4839, https://doi.org/10.5194/amt-13-4791-2020.

Sha, M. K., and Coauthors, 2021: Validation of methane and carbon monoxide from sentinel-5 precursor using TCCON and NDACC-IRWG stations. *Atmospheric Measurement Techniques*, **14**, 6249–6304, https://doi.org/10.5194/amt-14-6249-2021.

Tada, R., H. B. Zheng, and P. D. Clift, 2016: Evolution and variability of the Asian monsoon and its potential linkage with uplift of the Himalaya and Tibetan Plateau. *Progress in Earth and Planetary Science*, **3**, 4, https://doi.org/10.1186/s40645-016-0080-y.

Tu, Q. S., and Coauthors, 2020: Intercomparison of atmospheric CO_2 and CH_4 abundances on regional scales in boreal areas using copernicus atmosphere monitoring service (CAMS) analysis, COllaborative carbon column observing network (COCCON) spectrometers, and Sentinel-5 Precursor satellite observations. *Atmospheric Measurement Techniques*, **13**, 4751–4771, https://doi.org/10.5194/amt-13-4751-2020.

Wunch, D., and Coauthors, 2011: The total carbon column observing network. *Philosophical Transactions of the Royal Society A: Mathematical, Physical and Engineering Sciences*, **369**, 2087–2112, https://doi.org/10.1098/rsta.2010.0240.

Wunch, D., G. C. Toon, V. Sherlock, N. M. Deutscher, C. Liu, D. G. Feist, and P. O. Wennberg, 2015: Documentation for the 2014 TCCON data release. Pasadena. Available from https://doi.org/10.14291/tccon.ggg2014.documentation.R0/1221662.

Wunch, D., and Coauthors, 2017: Comparisons of the orbiting carbon observatory-2 (OCO-2) X_{CO_2} measurements with TCCON. *Atmospheric Measurement Techniques*, **10**, 2209–2238, https://doi.org/10.5194/amt-10-2209-2017.

Yang, Y., and Coauthors, 2020: New ground-based Fourier-transform near-infrared solar absorption measurements of X_{CO_2}, X_{CH_4} and X_{CO} at Xianghe, China. *Earth System Science Data*, **12**, 1679–1696, https://doi.org/10.5194/essd-12-1679-2020.

Zhang, G. F., Z. T. Nan, L. Zhao, Y. J. Liang, and G. D. Cheng, 2021: Qinghai-Tibet Plateau wetting reduces permafrost thermal responses to climate warming. *Earth and Planetary Science Letters*, **562**, 116858, https://doi.org/10.1016/j.epsl.2021.116858.

Zhou, D. C., L. Hao, J. B. Kim, P. L. Liu, C. Pan, Y. Q. Liu, and G. Sun, 2019: Potential impacts of climate change on vegetation dynamics and ecosystem function in a mountain watershed on the Qinghai-Tibet Plateau. *Climatic Change*, **156**, 31–50, https://doi.org/10.1007/s10584-019-02524-4.

Zhou, M. Q., and Coauthors, 2016: Validation of TANSO-FTS/GOSAT X_{CO_2} and X_{CH_4} glint mode retrievals using TCCON data from near-ocean sites. *Atmospheric Measurement Techniques*, **9**, 1415–1430, https://doi.org/10.5194/amt-9-1415-2016.